Discover Medicine

RESEARCH Open Access

Real-time breath drug metabolic monitoring under stellate ganglion block with lidocaine: a proof-of-concept study

Zhihong Yin[1,2†], Wei Xiong[3†], Keda Zhang[4], Xin Luo[5], Ming Wei[3], Kapil Dev Singh[1,2], Urs Frey[1,2], Xue Li[5], Xia Feng[3*] and Pablo Sinues[1,2*]

[†]Zhihong Yin and Wei Xiong have contributed equally to this work.

*Correspondence:
Xia Feng
fengxia@mail.sysu.edu.cn
Pablo Sinues
pablo.sinues@unibas.ch
[1]Department of Biomedical Engineering, University of Basel, Basel-Land CH-4123, Switzerland
[2]University Children's Hospital Basel, Basel CH-4031, Switzerland
[3]Department of Anesthesiology, The First Affiliated Hospital of Sun Yat-sen University, Guangzhou 510080, Guangdong, China
[4]College of Pharmacy, Shenzhen Technology University, Shenzhen 518118, Guangdong, China
[5]Institute of Mass Spectrometry and Atmospheric EnvironmentGuangdong Provincial Key Laboratory of Speed Capability Research, Jinan University, Guangzhou 510632, Guangdong, China

Abstract

Background Stellate ganglion block (SGB) using lidocaine has been widely employed in clinical practice to manage sympathetic-mediated pain and other autonomic-related conditions. However, the systemic metabolic response to this procedure is incompletely understood.

Methods In this pilot study, we enrolled 28 participants—17 healthy volunteers and 11 patients with sympathetically maintained pain—to investigate real-time metabolic changes induced by lidocaine-based SGB. Each participant received a 5 mL injection of 1% lidocaine under ultrasound guidance at the stellate ganglion, and exhaled breath samples were collected immediately before- and 5–30 min post-procedure. High-resolution mass spectrometry coupled with secondary electrospray ionization (SESI-HRMS) was used to detect changes in breath-borne metabolites.

Results A total of 309 features were significantly altered (q-value < 0.01 and $|\text{mean}(\log_2 FC)| > 1.5$) following lidocaine injection, with 233 upregulated and 76 downregulated. Among the most pronounced changes were lidocaine-derived metabolites, including 2,6-Dimethylaniline (2,6-DMA) and 2-amino-3-methylbenzoate, confirming that SESI-HRMS can rapidly track drug metabolism via breath. Hierarchical clustering further revealed a subgroup of healthy volunteers exhibiting especially robust metabolic shifts, suggesting inter-individual variability. Besides drug-related signals, several endogenous pathways appeared modulated, as indicated by altered levels of acylcarnitines, amino-acid derivatives, monoterpenes, and short-chain aldehydes, commonly implicated in fatty-acid β-oxidation, branched-chain amino-acid catabolism, and sympathetic regulation.

Conclusions These findings highlight real-time breath analysis as a feasible approach to capture both drug-specific (e.g., lidocaine metabolites) and host metabolic responses to SGB. By demonstrating clear inter-individual differences, this study supports the potential for breath-based pharmacometabolomics in monitoring and possibly optimizing lidocaine-SGB interventions in clinical settings.

Keywords Stellate ganglion block, Lidocaine, VOCs, Breath metabolomics, SESI-HRMS

1 Introduction

Since the mid-1930s, Stellate ganglion block (SGB) has been widely conducted to treat sympathetic-mediated pain (SMP). Evidence-based indications span complex regional pain syndrome (CRPS), neuropathic pain, autonomic dysfunction (e.g., hyperhidrosis, post-traumatic stress disorder (PTSD)), vascular/circulatory disorders, immune-related conditions (e.g., sudden deafness, allergic rhinitis), and systemic syndromes (e.g., menopausal hot flashes, chemotherapy-induced insomnia) [1–7]. SGB is a sympathetic nerve block that decreases sympathetic tone by infiltrating the stellate ganglion with local anesthetics. Lidocaine is commonly used as a local anesthetic for SGB due to its safety, rapid onset of action and rapid metabolization [8]. Despite SGB has shown great clinical potential as an adjunct treatment modality, its underlying mechanism of action remains poorly understood. Additionally, a comprehensive understanding of individual systemic responses to lidocaine SGB may help identify subgroups of patients who are more likely to benefit substantially from the intervention [9]. This stratification could reduce the widespread and non-selective use of SGB and promote more targeted, personalized treatment [10]. Pharmacometabolomics is a key technology to precision medicine and is ideally suited to heterogeneous phenotypes of drug intervention response among patients [11].

Breath-guided pharmacometabolomics is an attractive approach due to its non-invasiveness and unlimited sampling possibilities, ideally suited to monitor temporal metabolic profiles [12–14]. The possibility of monitoring in real-time metabolic changes induced by drugs in exhaled breath, offers a novel opportunity to explore individual responses to medication. Thus, we have previously shown that breath metabolomics enables to track systemic response (including drugs and drug metabolites) to therapeutic intervention in real-time, in vivo and non-invasively [15–19].

In this pilot study, we extended this prior work to address the question of whether breath-based pharmacometabolomic could provide insights into the still poorly understood mechanism of action of lidocaine in SGB interventions, as well as to identify whether participants undergoing such intervention could be stratified according to their metabolic response.

2 Methods

2.1 Study participants

A total of 28 participants were enrolled in this study from December 2021 to June 2022 through a staged recruitment strategy, beginning with 17 healthy volunteers (7 males and 10 females; mean ± SD age, 27.1 ± 3.5 years) to establish baseline SGB-induced metabolic fingerprints in a disease-free context, where initial data preprocessing confirmed our ability to rapidly capture post-intervention breath volatile organic compounds (VOCs) changes. Followed by adding 11 patients with sympathetically maintained pain (3 males, 8 females; mean ± SD age, 41.8 ± 11.1 years) to assess whether VOCs profile differences post-SGB exist between pathological and physiological states, extending our methodological validation to clinical populations. None of the participants had allergy to lidocaine, skin defect and infection at the neck puncture site, bradyarrhythmia, history of insomnia, cardiovascularity-related and brain diseases, or took medication that affects the cardiovascular system. This study was registered in Chinese Clinical Trial (https://www.chictr.org.cn/), registration number is ChiCTR2100048570. The registrati

on date was 20,210,711 and the date of first participant enrollment was 20,211,226. This study has been approved by the Institutional Ethics Committee of Clinical Research and Animal Trails of the First Affiliated Hospital of Sun Yat-sen University ([2021]730-1). This study was performed in accordance with the Declaration of Helsinki and each participant signed an informed written consent.

2.2 Stellate ganglion block

All SGB procedures were performed under ultrasound guidance by senior anesthesiologists (with 15 years of experience), and the specific operation details are as described previously [20]. A high-frequency ultrasound probe (M-Turbo Sonosite, Fuji Film) was applied to the patient's neck region to visualize the area at the level C6 to C7 and a 21 Gauge needle (Stimuplex D, B.Braun, Melsungen, Germany) was real-time guided in an in-plane fashion until the tip of the needle punctured the prevertebral fascia between the carotid sheath and longus colli muscle (Supplemental material Fig. 1a). Then 5 mL 1% lidocaine was injected at the surface of longus colli muscle with normal push resistance after negative aspiration for no vascular puncture, and hypoechoic local anesthetic spread could be observed by ultrasound (Supplemental material Fig. 1b).

We used the presence of Horner syndrome as an indicator for the confirmation of successful SGB [21]. Horner Syndrome is mainly characterized by ipsilateral ptosis, pupil narrowing, blushing, elevated skin temperature, and anhidrosis. The key factor for judging adequate block in this study was ptosis in Horner's syndrome, which was the most common flag after SGB and appeared in almost 100% of SGB cases [22]. During the entire experiment, the occurrence of adverse reactions such as hoarseness of voice, numbness of the upper limbs, pneumothorax, hematoma, and dizziness was recorded [7].

2.3 Study protocol

Healthy volunteers were recruited from hospitals and universities and the patients were recruited from hospital outpatient clinics. One hour before the exhaled breath test, all participants were required to refrain from consuming food, alcoholic beverages, or soft

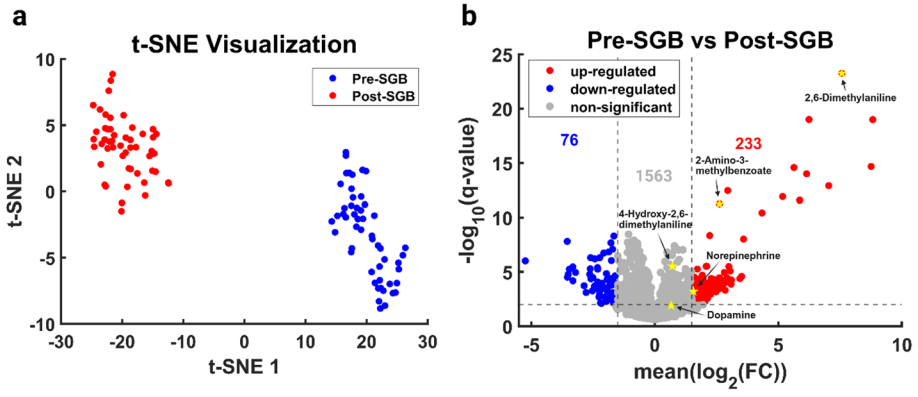

Fig. 1 SGB intervention with lidocaine induces rapid metabolic shifts in exhaled breath. (a) Two-dimensional t-SNE visualization of the 309 significant features ($q < 0.01$ and $|\text{mean}(\log_2 FC)| > 1.5$) from pre- vs. post-SGB breath samples ($n = 52$ pairs). Pre-SGB data (blue) cluster separately from post-SGB data (red), reflecting a clear metabolic response to lidocaine injection; (b) Volcano plot of all 1,872 retained features, highlighting these 309 significant changes. Red ($n = 233$) and blue ($n = 76$) circles represent features that were significantly up- or down-regulated, respectively, while non-significant features (grey) remain unchanged. Notable signals include 2,6-DMA and 2-amino-3-methylbenzoate—key metabolites in the known metabolism of lidocaine

drinks (except water), applying lipstick or lip balm, and using perfume in order to minimize the impact of confounding factors on the measurement. In addition, upon arrival at the breath testing laboratory, participants were asked to fill out a questionnaire regarding their illnesses, medication, alcohol and smoking history, as well as diet, sleep, and other relevant information over the past three days for follow-up data analysis. In the healthy volunteer group, the decision on which side of the cervical area to perform the first SGB intervention was made randomly using a random number generated by the software SPSS 22. The same procedure was repeated on the opposite side of the first intervention a week later. In the patient group, the SGB side was determined by the physician according to the patient's symptoms, and the side of subsequent intervention was maintained or adjusted according to the treatment effects of SGB. A baseline breath metabolomics measurement was performed before SGB intervention, and a follow-up test took place within 5–30 min after the onset of Horner's syndrome. Supplemental material Fig. 2 shows an overview of SGB intervention and exhaled breath dataset collection. In instances where two breath measurements were not completed in the healthy group, the main reasons were: (1) technical issues during the subject visit; and (2) participant withdrawal.

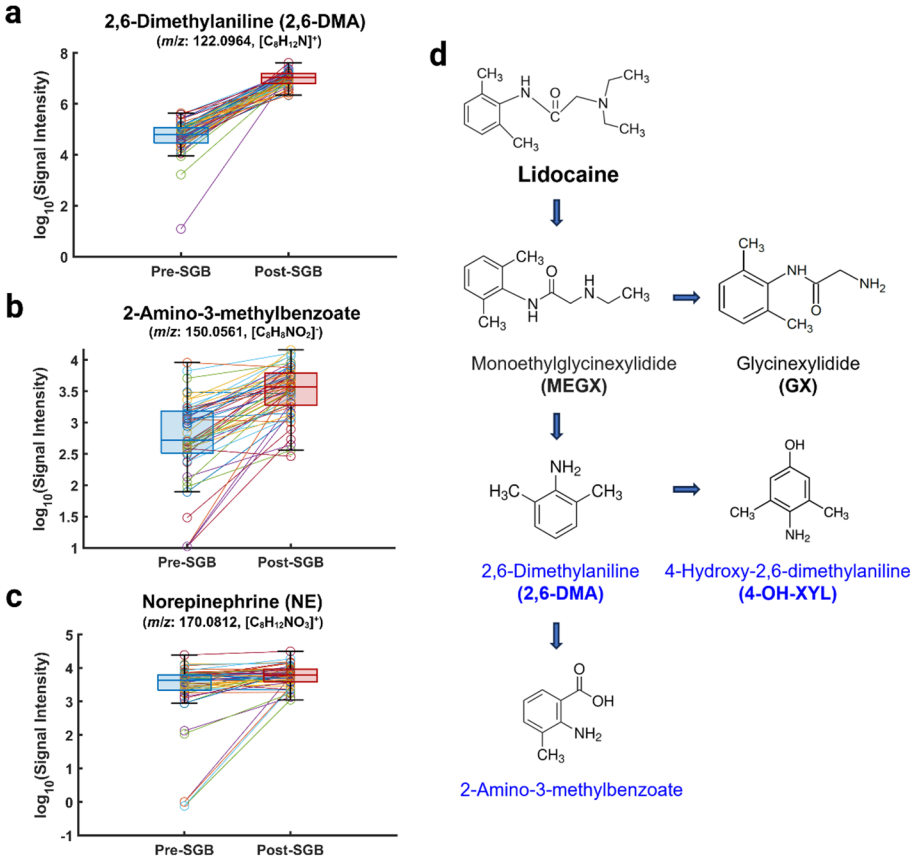

Fig. 2 a-c shows the stick plot for these three metabolites, whereby the overall increase at an individual level is observed. Supplemental material Fig. 5 shows the equivalent plots for the remaining two non-significant molecules (i.e., DP and 4-OH-XYL). Figure 2d shows Schematic representation of the known lidocaine metabolism leading to 2,6-DMA, 4-OH-XYL and 2-Amino-3-methylbenzoate

2.4 Real-time breath measurement

Real-time breath metabolomics fingerprints were accomplished in SESI-HRMS analytical platform located within hospital premises. The breath measurement procedures were carried out following the standardized operational procedures, as described in our previous protocol [23]. A breath test encompasses 12 replicate exhalations (six each in positive and negative ion mode). The time spent on a complete real-time breath analysis typically lasted around 10–15 min. Commercially disposable mouthpiece plastic with filter (MicroGard™, Vyaire Medical, USA; filters 99.98% of bacteria and 99.92% of viruses) were used in this study. To test the generalizability of the breath test for this clinical case, we used two different HRMS during the study: Q-Exactive and Exactive (Orbitrap MS, Thermo Fisher Scientific, Germany). The tuning parameters for the Q-Exactive were full scan, *m/z* range = 70–1000, resolution = 140,000, ion spray voltage = ± 2.8 kV, sheath gas flow = 60, auxiliary gas flow = 2, microscans = 2, capillary temperature = 275°. For Exactive were the same except for the resolution = 100,000. The sampling line and the ion chamber of the SESI source (Super SESI-QE, Fossiliontech, Spain) were heated to 130 °C and 90 °C, respectively to minimize metabolites adsorption onto the walls. The SESI nano-spray solution was water with 0.1% (v/v) formic acid and the nanoflow was induced by pressurizing the vial at 1.3 bar. During the study period, we performed quality control with 100 ppb of α-pinene standard gas in positive mode through the exhalation analysis platform before the first breath measurement of the day. Additionally, the weekly external calibration of MS was conducted using the commercially calibration solution (Pierce™ ESI Positive/Negative, Thermo Fisher Scientific, American).

2.5 Statistical analysis

Mass spectrometric RAW files were preprocessed using in-house C# console applications based on Thermo Fisher Scientific's RawFileReader (version 5.0.0.38) and MATLAB (R2022a; MathWorks Inc., USA). Representative spectra were generated by averaging scans during exhalation with CO_2 >3% to focus on end-tidal fractions. Mass spectra were calibrated using as reference peaks molecular formulae generated using the "seven golden rules" [24] present in at least 80% of the samples. Apodization was applied to remove artifact satellite peaks, and the centroid data set was binned with a tolerance of ± 1 ppm using MATLAB's *ksdensity* function. Pairs of positive and negative ion mode mass spectra from the same sample were fused. Subsequently, features present (i.e., signal intensity >0) in at least 60% of the samples were carried over, thereby dropping most sparse signals. The remaining zero values were imputed with the minimum signal intensity >0 detected across all measurements. ComBat algorithm (as implemented in R) was subsequently conducted to correct the batch effect induced by the two different mass spectrometers [25]. To assess changes before and after lidocaine injection, $\log_2$ fold change ($\log_2$FC) per participant was calculated, which was subsequently subjected to one-sample t-tests adjusting the resulting p-values for multiple comparisons using Storey's method [26]. Significant features were defined as $q < 0.01$ and the absolute value of mean($\log_2$FC) >1.5. t-distributed stochastic neighbor embedding (t-sne) and hierarchical cluster analysis were performed using *t-sne* and *clustergram* MATLAB built-in functions, respectively. A chi-square test was used to evaluate differences in participant subgroup composition (healthy volunteers vs. patients) among the identified clusters. Metabolite matching of the mass spectral features was mapped against the HMDB [27]

database using ± 1 ppm of mass tolerance for $[M + H]^+$ or $[M\text{-}H]^-$ ions (i.e., positive or negative mode).

3 Results

In this study, we enrolled 28 participants. Six participants underwent the SGB intervention using lidocaine once, whereas 22 received lidocaine up to four times (Supplemental material Fig. 2). The hallmark of successful stellate ganglion block is the presence of Horner's syndrome ipsilaterally [28]. All subjects in this study developed ipsilateral ptosis within 5–10 min post-procedure (Supplemental material Fig. 3). No adverse reactions were observed among all the participants. In this study, a total of n = 52 paired post-/pre-SGB breath samples were collected, resulting in N = 104 high resolution mass spectra (positive and negative ion mode combined sample-wise). The preprocessing workflow successfully corrected for experimental mass spectral inaccuracies of the raw data in both instruments, bringing down the mass accuracy well below ± 1 ppm (Supplemental material Fig. 4). Upon discarding sparse features (i.e., signal intensity >0 in less than 60% of the samples), the final data matrix dimensionality was reduced from 104 × 4,331 to 104 × 1,872 (samples-features). The high mass accuracy achieved (Supplemental material Fig. 4), allowed for a high-confidence mapping of these features against HMDB database (Online HMDB Mapping Results). As a result, 10,911 potential metabolites were listed.

A paired t-test was conducted on $\log_2$(Post-SGB/Pre-SGB), resulting in 309 significant ($q < 0.01$ and $|\text{mean}(\log_2 FC)| > 1.5$) features. A two-dimensional representation via t-sne of such changes in the exhaled metabolic profiles induced by SGB is shown in Fig. 1a, showing clearly two clusters corresponding to pre- and post-intervention across all participants. Further insights on the differential analysis were gathered by representing the data as a volcano plot (Fig. 1b), whereby 233/76 mass spectral features were up-/down-regulated upon lidocaine injection. Interestingly, the mapping against HMDB flagged five molecules associated with lidocaine pathways (i.e., Lidocaine (Antiarrhythmic) Action Pathway or Lidocaine (Local Anaesthetic) Action Pathway or Lidocaine (Local Anaesthetic) Metabolism Pathway). Namely, 2,6-Dimethylaniline (2,6-DMA) ($[M + H]^+$),

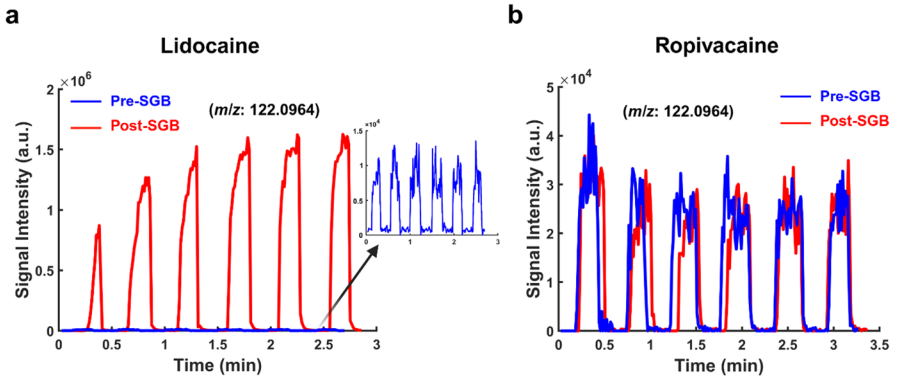

Fig. 3 Lidocaine-specific appearance of 2,6-dimethylaniline (2,6-DMA) in exhaled breath. (a) Representative time traces from six consecutive exhalations in a participant before (blue) and after (red) lidocaine-based SGB. A marked increase in signal intensity (by two orders of magnitude) indicates rapid generation of 2,6-DMA upon lidocaine metabolism. Inset shows a closer look at pre-SGB signals on the same timescale. (b) Equivalent measurements for a participant receiving ropivacaine-based SGB reveal no substantial change in signal intensity, suggesting that this metabolite arises specifically from lidocaine rather than from a generalized response to the SGB procedure

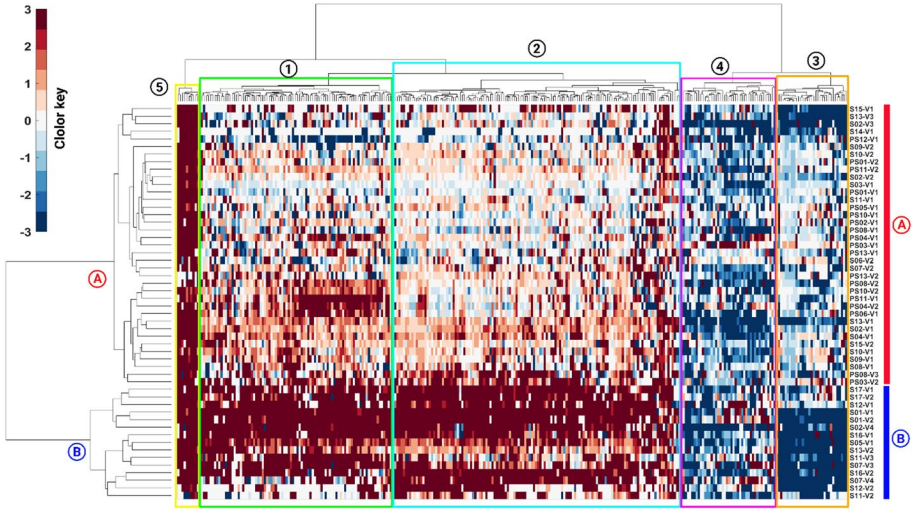

Fig. 4 Hierarchical clustering analysis of significantly altered exhaled metabolites reveals distinct response patterns to lidocaine SGB. Clustering was performed on the 309 significantly changed features (q-value < 0.01, |mean(log_2FC)| > 1.5). Each column represents one altered metabolite (labeled by its molecular formula), and each row corresponds to a specific subject and visit (e.g., "PS01-V2" for Patient Subject 01, Visit 2; "S03-V1" for Healthy Subject 03, Visit 1). Three main clusters of upregulated metabolites (clusters 1, 2, and 5) and two clusters of down-regulated metabolites (clusters 3 and 4) are clearly observed. At the participant level, hierarchical clustering also segregates subjects into two major groups (Clusters A and B), with Cluster B comprised solely of healthy volunteers exhibiting stronger metabolic shifts post-injection. See Online Supplemental Datasets 1 and 2 for detailed cluster assignments and participant information

4-Hydroxy-2,6-dimethylaniline (4-OH-XYL) ($[M+H]^+$), 2-Amino-3-methylbenzoate ($[M-H]^-$), Dopamine (DP) ($[M+H]^+$) and Norepinephrine (NE) ($[M+H]^+$). In all five compounds the trend found was towards upregulation (i.e., an increase in breath concentration upon lidocaine injection). However, only 2,6-DMA, 2-Amino-3-methylbenzoate and NE remained significant.

Figure 2 Lidocaine-derived metabolites and endogenous catecholamines increase after SGB. (a–c) Stick plots of three significantly upregulated features (q < 0.01, |mean(log_2FC)| >1.5) showing pre-SGB (blue) vs. post-SGB (red) intensities on a log_{10}scale for each participant. (a) 2,6-DMA, (b) 2-amino-3-methylbenzoate, and (c) Norepinephrine. The boxes indicate the median and interquartile range, and whiskers represent the full range of measurements; (d) Proposed pathway of lidocaine metabolism. Lidocaine undergoes sequential N-dealkylations to form monoethylglycinexylidide (MEGX) and glycinexylidide (GX), ultimately yielding 2,6-DMA, which can be further hydroxylated to 4-OH-XYL or ring-cleaved into 2-amino-3-methylbenzoate.

In this study, we relied on exact mass measurements to determine unique molecular formulas, which we then mapped to the Human Metabolome Database (HMDB) for preliminary structural assignments at level 3 confidence [29]. To further validate our annotation of 2,6-DMA, we compared SGB interventions performed using ropivacaine instead of lidocaine. As shown in Figs. 3 and 6-DMA did not increase when ropivacaine was used, thus reinforcing the conclusion that 2,6-DMA arises specifically from lidocaine metabolism rather than from a general response to SGB.

To gain further insight into the existence of potential different responses to the medication across all participants as well as associations at the molecular level, we conducted a hierarchical clustering analysis for 309 significant features (Fig. 4). At the metabolite level, hierarchical clustering analysis identifies three upregulated clusters (1, 2, and 5)

and two downregulated clusters (3 and 4), as shown in Fig. 4, with a detailed list of these compounds provided in Online Dataset 1. At the participant level, hierarchical clustering analysis reveals two distinct groups: Cluster A includes all patients along with some healthy volunteers, whereas Cluster B comprises approximately one-third of the measurements, representing exclusively healthy volunteers (see Online Dataset 2).

4 Discussion

To the best of our knowledge, this is the first pharmacometabolomics study that attempts to elucidate the systemic impact of lidocaine SGB on the human body from the perspective of exhaled metabolites. The results of this study indicate that SGB lidocaine induced significant changes in breath metabolites could be rapidly captured by the SESI-HRMS real-time online breath analysis platform within 5 min after the Horner effect appears.

A total of 309 mass spectral features changed significantly after SGB intervention, with 233 upregulated and 76 downregulated following lidocaine injection. These altered expiratory metabolites appear to be driven by lidocaine metabolism and the successful activation of SGB. Among the significantly changed compounds, we identified two clear lidocaine-derived metabolites: 2,6-DMA and 2-amino-3-methylbenzoate. A third metabolite, 4-OH-XYL, was also detected at higher levels, although it did not meet our strict significance threshold (mean $\log_2$FC = 0.7, $q < 0.01$). These observations align with the known metabolic pathway of lidocaine, which undergoes cytochrome P450-mediated amide bond cleavage to form 2,6-DMA (Fig. 2d) and smaller peptides (e.g., monoethylglycinexylidide [30]). Once formed, 2,6-DMA can be further hydroxylated at the para-position to yield 4-OH-XYL, a more polar metabolite that is primarily excreted in the urine. Our real-time breath analysis effectively traces changes in 2,6-DMA in a non-invasive manner, even though up to 75% of this metabolite is ultimately excreted in the urine as 4-OH-XYL [31]. Notably, 2,6-DMA has been identified as a carcinogen in rats [32], though no definitive link to human cancers has been established. Compared with conventional liquid chromatography-mass spectrometry (LC–MS) or gas chromatography-mass spectrometry (GC–MS) techniques [33–36], our method overcomes the need for invasive sampling and extensive preprocessing, enabling more efficient and real-time monitoring of 2,6-DMA. Additionally, our data suggest the presence of 2-amino-3-methylbenzoate, a product potentially arising from ring-cleavage or partial oxidation of the methyl-substituted ring on DMA, resulting in a benzoic acid moiety. Although 2-amino-3-methylbenzoate is not typically reported among the major lidocaine metabolites, its formation is chemically plausible through di- or tri-hydroxylation steps followed by rearrangement, a process well-described in aromatic amine metabolism [37]. Collectively, these findings highlight a deeper oxidative capacity of lidocaine metabolism than previously characterized, shedding light on additional pathways that might modulate the drug's pharmacokinetics and toxicological profile.

Whether a circulating metabolite will eventually be exhaled in breath largely depends on its ability to diffuse from blood to air [38]. As in our previous studies [39], we used the apparent blood-brain barrier permeability coefficient (PC_{BBB}) as an evaluation for the ability of these drug-derived compounds to penetrate the cell membrane and calculated it using the linear free-energy relationship (LFER) equation provided by Abraham et al. [40]. The independent variables used in the calculation equations are shown in Supplemental material Table 1. The calculation results of lidocaine and its four main

metabolites are shown in Supplemental material Table 2. Under physiological conditions (blood, pH 7.4), 2,6-DMA has the highest apparent PC_{BBB} (5.19×10^{-4} cm s^{-1}), which is close to carbon dioxide (CO_2, $PC_{BBB} = 4.4 \times 10^{-3}$ cm s^{-1}) [41]. CO_2 is considered to pass freely through biological membranes. And the tissue binding (/retention) ability of 2,6-DMA is moderate, which does not affect its rapid diffusion within the system. In addition, 2,6-DMA has a water/air partition coefficient ($K_{water/air}$) of 1.01×10^4, and its ability to diffuse from water to air is much higher than that of lidocaine and other metabolites. In addition, 2,6-DMA 4-OH-XYL and 2-amino-3-methylbenzoate exist mainly in the form of neutral molecules (Depending on the pKa) in lung lining fluid (LLF), while lidocaine, MEGX, and GX exist mainly in the form of ions (ions cannot be distributed into the air). This means that 2,6-DMA is more easily distributed into exhaled air in the form of gas molecules. In summary, compared with lidocaine and other metabolites, 2,6-DMA has a higher transport capacity from blood to breath and is easier to detect in exhaled breath.

In addition to these three drug-derived metabolites, our study shows a significant increase in norepinephrine (mean $\log_2FC = 1.6$, $q << 0.05$; Fig. 2c) and a non-significant rise in dopamine (mean $\log_2FC = 0.7$, $q < 0.05$; Supplemental material Fig. 5) ~ 15 min after lidocaine injection. We previously found these two metabolites in exhaled breath associated with pediatric patients not responding to antiseizure medications [15]. In this context, we hypothesize that this initial spike likely reflects an acute stress response [42, 43] or incomplete stellate ganglion blockade during the early post-injection phase. Acute stress activates the sympathetic nervous system, leading to the release of norepinephrine from nerve cells in the brainstem and spinal cord. Dopamine, a precursor to norepinephrine, is also released, contributing to the overall stress response.

Our analysis reveals that SGB intervention with lidocaine encompasses a broader metabolic response beyond the five compounds discussed so far. The cluster analysis presented in Fig. 4 and Online Dataset 1 reveals a distinct cluster (number 5) of exhaled molecules with a high abundance ($Log_2FC > 3$) across all participants, which includes 2,6-DMA. These very stark changes and the presence of 2,6-DMA ($C_8H_{11}N$) suggest that these signals could potentially be drug-derived. For example, higher-oxygen derivatives ($C_8H_{13}O_4N$, $C_8H_{13}O_5N$, $C_8H_{11}O_3N$) suggest downstream oxidative transformations on the aromatic ring, consistent with documented pathways of aromatic amine hydroxylation and ring-cleavage. However, further work remains to validate this hypothesis.

Clusters 1 and 2 show very similar metabolomic responses to lidocaine injection, with both exhibiting an overall upregulation in a subgroup of exclusively healthy volunteers (i.e., cluster B). Biochemically, both clusters contain numerous acylcarnitines—ranging from medium-chain (heptanoyl, octenoyl) to more diverse, partially oxidized species—and a variety of amino-acid derivatives. This pattern strongly suggests heightened activity in fatty-acid β-oxidation and branched-chain amino-acid catabolism pathways. Furthermore, the presence of catecholamine-related metabolites in Cluster 1 underscores the intervention's potential impact on neurotransmitter metabolism, consistent with lidocaine SGB's known effects on sympathetic regulation. Meanwhile, Cluster 2 exhibits several drug-like and xenobiotic compounds, indicating that these metabolite clusters integrate not only endogenous processes, but also exogenous amine-containing molecules influenced by stellate ganglion blockade.

In contrast to Clusters 1 and 2, which exhibited overall upregulation, Clusters 3 and 4 show a global downregulation of their constituent metabolites—most prominently in healthy volunteers. Both clusters feature short-chain aldehydes, hydrocarbons, and low-molecular-weight volatiles (e.g., pentanal, isovaleraldehyde, nonenes, dodecenes) alongside various terpene-like or lipid-derived molecules (anhydroretinol, ent-16-kaurene, cembrene), as well as an extensive collection of monoterpenes (limonene, α-pinene, sabinene, phellandrene) and aromatic aldehydes (cuminaldehyde, anisole, methylbenzaldehydes). Many of these compounds arise from plant-derived dietary components, environmental exposures, or lipid peroxidation, suggesting that the SGB-induced metabolic adjustments—potentially via altered sympathetic outflow or modified hepatic processing—could reduce the circulating levels of these exogenous or semi-exogenous molecules. The especially pronounced downregulation in the healthy subgroup further indicates that baseline metabolic status or lifestyle factors may play a role in how these externally sourced compounds are metabolized post-lidocaine SGB.

At the participant level, the hierarchical clustering analysis showed that one group comprising around one-third of the participants—exclusively healthy volunteers (Cluster B)—displayed a strong alteration in expiratory metabolites, while the remaining healthy volunteers and patients (Cluster A) had only moderate changes. A subsequent chi-square test ($\chi^2 = 12.14$, $p = 4.9 \times 10^{-4}$) confirmed that these two clusters differ significantly in their proportion of healthy and patient participants, underscoring the distinct metabolic profiles observed in Cluster B's healthy-only subgroup compared to the mixed group in Cluster A. This finding suggests that sympathetic pain may influence lidocaine metabolism or VOC patterns, although such an effect remains to be definitively proven. Notably, our previous work has identified distinct clusters of responders to inhaled medications [19], hinting that the presence of different metabolic phenotypes in response to SGB could similarly explain why patients and healthy volunteers diverge after lidocaine administration. Also on the note, it can be observed how most of the participants undergoing repeated measurements tend to cluster together (e.g., patient PS01 or healthy volunteer S01). This suggests that the response to the medication for these participants is very similar across interventions. In contrast, a minority of participants show a large variability from one measurement to the next (e.g., visit 4 of S02; Supplemental material Fig. 6), suggesting a distinct response to lidocaine over the sequential series of interventions. In addition, we evaluated whether there were significant differences between left- and right-side neck interventions. However, our analysis did not reveal any notable or substantial differences (Supplemental material Fig. 7), which aligns with most studies on the differential effects of left- versus right-sided SGB on ventricular function and the cardiovascular system [44, 45].

Finally, our real-time detection of 2,6-DMA and other lidocaine-derived metabolites highlights the potential of breath analysis as a rapid, noninvasive tool for tracking lidocaine exposure and monitoring potential toxicity. Beyond lidocaine metabolism, changes in endogenous VOCs could serve as markers of treatment response—particularly if further research confirms correlations between specific exhaled metabolites and pain relief duration or analgesic efficacy, paving the way for personalized analgesia strategies. In prior studies, we harnessed breath-based pharmacometabolomics to track propofol metabolism during anesthesia [17], inhaled medications [19], insulin therapy [18], and antiseizure medications [15], correlating exhaled biomarkers with clinical outcomes

(e.g., treatment response) and adverse effects. These findings underscore the broader applicability of this noninvasive approach, suggesting that a similar framework could be extended to lidocaine-based regional anesthesia for more personalized and safer analgesic strategies. While the findings here are encouraging, larger, longitudinal studies will be essential to validate these biomarker-based approaches and firmly establish breath analysis as a routine clinical tool for guiding lidocaine dosing, enhancing patient safety, and improving therapeutic outcomes.

While this study provides promising evidence for the feasibility of breath-based pharmacometabolomics in assessing SGB interventions with lidocaine, several limitations must be acknowledged. First, the patient sample size was relatively small, restricting our ability to generalize the findings or to determine whether breath analyses can reliably predict which individuals will benefit most from SGB. Second, the follow-up data was limited, preventing a thorough evaluation of both the long-term treatment outcomes and potential side effects. Further research is also required to determine if these breath-based findings extend to other lidocaine-based regional anesthesia techniques, given systemic lidocaine metabolism yet potentially distinct physiological effects of different block approaches. Future studies should enroll larger patient cohorts, systematically monitor clinical responses at multiple time points, and collect corresponding breath samples for extended metabolomic profiling. Lastly, the inability to identify all significantly altered metabolites underscores the current constraints of mass spectrometry, including the lack of robust MS/MS data and limited breath-metabolite databases. Overcoming these analytical gaps will be essential for improving compound annotation and strengthening the interpretability of breath-based metabolomic results.

5 Conclusions

By employing SESI-HRMS for real-time breath analysis, this pilot study demonstrates that lidocaine-based stellate ganglion block (SGB) induces rapid and measurable alterations in exhaled metabolites. Among these were lidocaine-derived compounds (e.g., 2,6-DMA), confirming that the technique can trace drug metabolism in a noninvasive manner. In addition, multiple endogenous pathways appear to be modulated, as evidenced by significant shifts in acylcarnitines, amino-acid derivatives, short-chain aldehydes, and monoterpenes—molecules often linked to fatty-acid β-oxidation, branched-chain amino-acid catabolism, and sympathetic regulation. Hierarchical clustering uncovered a subgroup of healthy volunteers exhibiting especially pronounced changes, suggesting inter-individual variability in SGB response. Collectively, these observations underscore the feasibility of breath-based pharmacometabolomics for capturing both drug-specific and host metabolic pathways affected by lidocaine SGB. Future work with larger cohorts and extended follow-up is warranted to establish whether such metabolic signatures can further refine patient monitoring and treatment strategies.

Abbreviations

SGB	Stellate ganglion block
SESI-HRMS	Secondary electrospray ionization high-resolution mass spectrometry
SMP	Sympathetic-mediated pain
CRPS	Complex regional pain syndrome
PTSD	Post-traumatic stress disorder
VOCs	Volatile organic compounds
2,6-DMA	2,6-Dimethylaniline
MEGX	Monoethylglycinexylidide
GX	Glycinexylidide

NE	Norepinephrine
DP	Dopamine
4-OH-XYL	4-Hydroxy-2,6-dimethylaniline
LC–MS	Liquid chromatography-mass spectrometry
GC–MS	Gas chromatography-mass spectrometry
PC_{BBB}	Blood-brain barrier permeability coefficient
LFER	Linear free-energy relationship
$K_{water/air}$	Water/air partition coefficient
LLF	Lung lining fluid

Supplementary Information

The online version contains supplementary material available at https://doi.org/10.1007/s44337-025-00498-0.

Supplementary Material 1

Supplementary Material 2

Supplementary Material 3

Supplementary Material 4

Acknowledgements
All the authors gratefully acknowledge all our healthy volunteers and patients for their cooperation throughout the study period.

Author contributions
Study conception and design: ZHY, WX, PS, XF, XLi. Data acquisition, analysis, interpretation: ZHY, WX, KDZ, WM, XLuo, KDS, PS. Writing of the original draft: ZHY, WX. Review, editing and final approval of the manuscript: all authors.

Funding
Open access funding provided by University of Basel. PS received funding from Fondation Botnar (Switzerland) and the Swiss National Science Foundation (PCEGP3_181300). National Natural Science Foundation of China (No.: 22122603, 82371189, 82071224, 82301354); Guangdong Major Project of Basic and Applied Basic Research (No.: 22022A1515010398, 023B0303000013).

Data availability
All data supporting the findings of this study are included within the article and its Supplementary Information. The anonymized mass spectrometry data collected in this study is publicly available at DOI: 10.17632/82w4m2nh39.1.

Declarations

Ethics approval and consent to participate
This study was registered in Chinese Clinical Trial (https://www.chictr.org.cn/), registration number is ChiCTR2100048570. The registration date was 20210711 and the date of first participant enrollment was 20211226. This study has been approved by the Institutional Ethics Committee of Clinical Research and Animal Trails of the First Affiliated Hospital of Sun Yat-sen University ([2021]730-1). This study was performed in accordance with the Declaration of Helsinki and each participant signed an informed written consent.

Consent for publication
Informed written consent for publication of anonymized data was obtained from all participants included in the study.

Competing interests
PS is cofounder of Deep Breath Intelligence AG (Switzerland), which develops breath-based diagnostic tools. KS is consultant for Deep Breath Intelligence AG (Switzerland). All other authors declare no conflict of interest.

Received: 7 March 2025 / Accepted: 18 September 2025
Published online: 05 October 2025

References

1. Rae Olmsted KL, et al. Effect of stellate ganglion block treatment on posttraumatic stress disorder symptoms: A randomized clinical trial. JAMA Psychiatry. 2020;77(2):130–38. https://doi.org/10.1001/jamapsychiatry.2019.3474.
2. Kirkpatrick K, Khan MH, Deng Y, Shah KB. A review of stellate ganglion block as an adjunctive treatment modality. Cureus. 2023;15(2):e35174. https://doi.org/10.7759/cureus.35174.
3. Chauhan G, Upadhyay A, Khanduja S, Emerick T. Stellate ganglion block for anosmia and dysgeusia due to long COVID. Cureus. 2022;14(8):e27779. https://doi.org/10.7759/cureus.27779.
4. Sinofsky A, Sharma T, Wright T. Stellate ganglion block for debilitating photophobia secondary to Trigeminal, postherpetic neuralgia. Pain Pract. 2016;16(7):E99–102. https://doi.org/10.1111/papr.12471.
5. Haest K, et al. Stellate ganglion block for the management of hot flashes and sleep disturbances in breast cancer survivors: an uncontrolled experimental study with 24 weeks of follow-up. Ann Oncol. 2012;23(6):1449–54. https://doi.org/10.1093/annonc/mdr478.

6. Luo G, et al. The therapeutic effect of stellate ganglion block on facial nerve palsy in patients with type 2 diabetes mellitus. Eur Neurol. 2015;74(1–2):112–7. https://doi.org/10.1159/000435834.
7. Goel V, et al. Complications associated with stellate ganglion nerve block: a systematic review. Reg Anesth Pain Med. 2019;44(6):669. https://doi.org/10.1136/rapm-2018-100127.
8. Weinberg L. Pharmacokinetics and pharmacodynamics of lignocaine: A review. World J Anesthesiol. 2015;4(2). https://doi.org/10.5313/wja.v4.i2.17.
9. Castro I, Carvalho P, Vale N, Monjardino T, Mourão J. Systemic Anti-Inflammatory effects of intravenous Lidocaine in surgical patients: A systematic review and Meta-Analysis. J Clin Med 2023; 12(11).
10. Horvat S, Staffhorst B, Cobben JMG. Intravenous Lidocaine for treatment of chronic pain: A retrospective cohort study. J Pain Res. 2022;15:3459–67. https://doi.org/10.2147/JPR.S379208.
11. Elbadawi-Sidhu M. Pharmacometabolomics as the key to personalised medicine. Drug Target Rev. 2016;3:22–5.
12. Martinez-Lozano Sinues P, Zenobi R, Kohler M. Analysis of the exhalome: a diagnostic tool of the future. Chest. 2013;144(3):746–49. https://doi.org/10.1378/chest.13-1106.
13. Miekisch W, Schubert JK, Noeldge-Schomburg GF. Diagnostic potential of breath analysis–focus on volatile organic compounds. Clin Chim Acta. 2004;347(1–2):25–39. https://doi.org/10.1016/j.cccn.2004.04.023.
14. Li X, et al. Drug pharmacokinetics determined by Real-Time analysis of mouse breath. Angew Chem Int Ed Engl. 2015;54(27):7815–8. https://doi.org/10.1002/anie.201503312.
15. Singh KD, et al. Personalised therapeutic management of epileptic patients guided by pathway-driven breath metabolomics. Commun Med. 2021;1(1):21. https://doi.org/10.1038/s43856-021-00021-3.
16. Gaugg MT, et al. Metabolic effects of inhaled salbutamol determined by exhaled breath analysis. J Breath Res. 2017;11(4):046004. https://doi.org/10.1088/1752-7163/aa7caa.
17. Zeng J et al. Breath analysis of Propofol and associated metabolic signatures: A pilot study using secondary electrospray ionization High-Resolution mass spectrometry. Anesthesiology. 9900.
18. Awchi MDSK, Brenner SB, Burckhardt M-A, HM, Zeng J, Datta ANFU. Zumsteg U, P SGaS. Metabolic trajectories of diabetic ketoacidosis onset described by breath analysis. Front Endocrinol. 2024.
19. Zeng J, et al. Pharmacometabolomics via real-time breath analysis captures metabotypes of asthmatic children associated with salbutamol responsiveness. iScience. 2024;27(12). https://doi.org/10.1016/j.isci.2024.111446.
20. Gofeld M, Bhatia A, Abbas S, Ganapathy S, Johnson M. Development and validation of a new technique for ultrasound-guided stellate ganglion block. Reg Anesth Pain Med. 2009;34(5):475–9. https://doi.org/10.1097/AAP.0b013e3181b494de.
21. Winnie AP, Ramamurthy S, Durrani Z, Radonjic R, Shaker MH. Pharmacologic Reversal of Horner's Syndrome Following Stellate Ganglion Block. Anesthesiology. 1974;41(6).
22. Abdi S, Yang Z. A novel technique for experimental stellate ganglion block in rats. Anesth Analg. 2005;101(2).
23. Gisler A, et al. An interoperability framework for multicentric breath metabolomic studies. iScience. 2022;25(12):105557. https://doi.org/10.1016/j.isci.2022.105557.
24. Kind T, Fiehn O. Seven golden rules for heuristic filtering of molecular formulas obtained by accurate mass spectrometry. BMC Bioinf. 2007;8(1):105. https://doi.org/10.1186/1471-2105-8-105.
25. Johnson WE, Li C, Rabinovic A. Adjusting batch effects in microarray expression data using empirical Bayes methods. Biostatistics. 2007;8(1):118–27. https://doi.org/10.1093/biostatistics/kxj037.
26. Storey JD. A direct approach to false discovery rates. J Roy Stat Soc B. 2002;64(3):479–98. https://doi.org/10.1111/1467-9868.00346.
27. Wishart DS, et al. HMDB 5.0: the human metabolome database for 2022. Nucleic Acids Res. 2022;50(D1):D622–31. https://doi.org/10.1093/nar/gkab1062.
28. Son MK, et al. The effects of local anesthetic distribution on symptoms using ultrasound image after stellate ganglion block. Korean J Anesthesiol. 2009;57(5):579–83. https://doi.org/10.4097/kjae.2009.57.5.579.
29. Schymanski EL, et al. Identifying small molecules via high resolution mass spectrometry: communicating confidence. Environ Sci Technol. 2014;48(4):2097–8. https://doi.org/10.1021/es5002105.
30. Tucker GT, PHARAMACOKINETICS OF LOCAL ANAESTHETICS. Br J Anaesth. 1986;58(7):717–31. https://doi.org/10.1093/bja/58.7.717.
31. Sellers G, et al. Pharmacokinetics of Lidocaine in serum and milk of mature Holstein cows. J Vet Pharmacol Ther. 2009;32(5):446–50. https://doi.org/10.1111/j.1365-2885.2009.01061.x.
32. Kirkland D, et al. Further investigations into the genotoxicity of 2,6-xylidine and one of its key metabolites. Regul Toxicol Pharmacol. 2012;62(1):151–9. https://doi.org/10.1016/j.yrtph.2011.08.010.
33. Puente NW, Josephy PD. Analysis of the Tidocaine metabolite 2,6-Dimethylaniline in bovine and human milk. J Anal Toxicol. 2001;25(8):711–15. https://doi.org/10.1093/jat/25.8.711.
34. Bebawy LI, Elghobashy MR, Abbas SS, Shokry RF. Chromatographic determination of aminoacridine hydrochloride, Lidocaine hydrochloride and Lidocaine toxic impurity in oral gel. J Chromatogr Sci. 2016;54(4):492–9. https://doi.org/10.1093/chromsci/bmv170.
35. Headley JV, Maxwell DB, Swyngedouw C, Purdy JR. Determination of combined residues of Metalaxyl and 2,6-Dimethylaniline metabolites in urine bygas Chromatography/Mass spectrometry. J AOAC Int. 2020;79(1):117–23. https://doi.org/10.1093/jaoac/79.1.117.
36. Marisetti VM, Katari NK. Development and validation of RP-UPLC method for 2,6-Dimethylaniline, its Isomers, and related compounds using design of experiments. Chromatographia. 2021;84(4):359–69. https://doi.org/10.1007/s10337-021-04014-1.
37. Nelson SD, Pearson PG. Covalent and noncovalent interactions in acute lethal cell injury caused by chemicals. Annu Rev Pharmacol Toxicol. 1990;30(30, 1990):169–95. https://doi.org/10.1146/annurev.pa.30.040190.001125.
38. Lopez-Lorente CI, Awchi M, Sinues P, Garcia-Gomez D. Real-time pharmacokinetics via online analysis of exhaled breath. J Pharm Biomed Anal. 2021;205:114311. https://doi.org/10.1016/j.jpba.2021.114311.
39. Chen X, et al. Online Real-Time monitoring of exhaled breath particles reveals unnoticed transport of nonvolatile drugs from blood to breath. Anal Chem. 2021;93(12):5005–08. https://doi.org/10.1021/acs.analchem.1c00509.
40. Abraham MH. The permeation of neutral Molecules, Ions, and ionic species through membranes: brain permeation as an example. J Pharm Sci. 2011;100(5):1690–701. https://doi.org/10.1002/jps.22404.

41. Friis ML, Paulson OB, Hertz MM. Carbon dioxide permeability of the blood-brain barrier in man: the effect of Acetazolamide. Microvasc Res. 1980;20(1):71–80. https://doi.org/10.1016/0026-2862(80)90020-5.
42. Bloomfield MAP, McCutcheon RA, Kempton M, Freeman TP, Howes O. The effects of psychosocial stress on dopaminergic function and the acute stress response. eLife. 2019;8:e46797. https://doi.org/10.7554/eLife.46797.
43. Finlay JM, Zigmond MJ, Abercrombie ED. Increased dopamine and norepinephrine release in medial prefrontal cortex induced by acute and chronic stress: effects of diazepam. Neuroscience. 1995;64(3):619–28. https://doi.org/10.1016/0306-4522(94)00331-X.
44. Lobato EB, Kern KB, Paige GB, Brown M, Sulek CA. Differential effects of right versus left stellate ganglion block on left ventricular function in humans: an echocardiographic analysis. J Clin Anesth. 2000;12(4):315–18. https://doi.org/10.1016/S0952-8180(00)00158-6.
45. de la Puente K, Gómez Perez MA, Roqueta C, Fischer L. Effects on hemodynamic variables and echocardiographic parameters after a stellate ganglion block in 15 healthy volunteers. Auton Neurosci. 2016;197:46–55. https://doi.org/10.1016/j.autneu.2016.04.002.

Publisher's note